Article

# Semiconductor Rings Fabricated by Self-Assembly of Nanocrystals

Bin Liu, and Hua Chun Zeng

*J. Am. Chem. Soc.*, **2005**, 127 (51), 18262-18268• DOI: 10.1021/ja055734w • Publication Date (Web): 02 December 2005



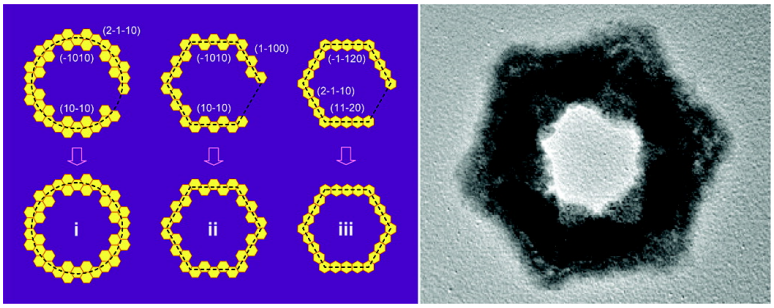


## More About This Article

Additional resources and features associated with this article are available within the HTML version:

- Supporting Information
- Links to the 28 articles that cite this article, as of the time of this article download
- Access to high resolution figures
- Links to articles and content related to this article
- Copyright permission to reproduce figures and/or text from this article

View the Full Text HTML

J|A|C|S
ARTICLES
Published on Web 12/02/2005

# Semiconductor Rings Fabricated by Self-Assembly of Nanocrystals

Bin Liu and Hua Chun Zeng*

*Contribution from the Department of Chemical and Biomolecular Engineering, Faculty of Engineering, National University of Singapore, 10 Kent Ridge Crescent, Singapore 119260*

Received August 22, 2005; E-mail: chezhc@nus.edu.sg

***Abstract:*** Three types of nonlinear organization schemes for creating ringlike semiconductors have been elucidated with the self-assembly of nanocrystals in aqueous phase under one-pot conditions. The synthetic architecture is based on morphological controls of primary nanocrystals which possess an intrinsic hexagonal symmetry. As most semiconducting materials have similar hexagonal (or cubic) crystal symmetries, in principle, the self-assembling processes revealed in this work should be extendable to other semiconductor nanocrystals.

## Introduction

Because of increasing structural complexity and demanding precision control, nonlithographic synthesis of functional ringlike objects in strict circular, oval, or polygonal forms may represent a next challenge of nanofabrication,[1−4] in addition to currently investigated zero- and one-dimensional (0D and 1D) materials such as nanoparticles, core−shells, rods, ribbons, wires, and helixes.[5−16] Concerning their unique structural features and new properties generated with ring cavities, several attempts have been made for preparations of meso- or nanoscopic ringlike structures over the past few years.[1−4] In particular, carbon nanotube rings,[1] zinc oxide coils and hexagonal rings,[2,3] titanium dioxide, and polymeric rings have been prepared, respectively.[4] It is noted that in all these studies, the ringlike structures were either reconfigured from a single piece of raw material or grown directly onto soft or hard templates, followed by template removal.[1−4] Fabrication of free-standing ringlike objects from small building blocks via self-organizing means, nonetheless, has so far remained unsuccessful, although hierarchical self-assembly has been well conceived to play a central role in the "bottom-up" paradigm.[17−21]

Organizing low-dimensional nanomaterials into larger structures through an underlying process called "oriented attachment" has been realized in recent years, where preformed primary crystallites can be joined together into larger ones if their crystallographic requirements are fulfilled.[22,23] Starting with nanocrystallites (0D), for example, nanorods (1D),[24,25] nanosheets (2D),[24,26] and mesoscale and/or nanoscale hollow spheres and polyhedrons (3D)[27,28] have been elucidated very recently. Herein, we will demonstrate that, in addition to the known linear alignment of nanocrystals,[22−28] a nonlinear (i.e., turning) 1D arrangement of nanocrystals can also be attained with the "fusion" of nanocrystals. In this work, meso- and nanoscopic ringlike structures of semiconductor cadmium sulfide (CdS) have been prepared via self-assembly of nanocrystals. The synthetic architecture is based on morphological controls of attached primary nanocrystals under one-pot conditions. Three organizing schemes have been revealed for the first time for line-turning and curvature formation.

## Experimental Section

In a typical synthesis, 0.308 g of $Cd(NO_3)_2 \cdot 4H_2O$ (99%, Merck) and 0.076 g of thiourea (99%, Merck) were dissolved in 40.0 mL of deionized water. Then 0−1.0 g of ground 1,12-dodecanediamine (98%,

(1) (a) Liu, J.; Dai, H.; Hafner, J. H.; Colbert, D. T.; Smalley, R. E.; Tans, S. J.; Dekker, C. *Nature* **1997**, *385*, 780. (b) Martel, R.; Shea, H. R.; Avouris, P. *Nature* **1999**, *398*, 299. (c) Sano, M.; Kamino, A.; Okamura, J.; Shinkai, S. *Science* **2001**, *293*, 1299.
(2) Kong, X. Y.; Ding, Y.; Yang, R.; Wang, Z. L. *Science* **2004**, *303*, 1348.
(3) Li, F.; Ding, Y.; Gao, P.; Xin, X.; Wang, Z. L. *Angew. Chem., Int. Ed.* **2004**, *43*, 5238.
(4) Yan, F.; Goedel, W. A. *Angew. Chem., Int. Ed.* **2005**, *44*, 2084.
(5) Caruso, F.; Caruso, R. A.; Möhwald, H. *Science* **1998**, *282*, 1111.
(6) Göltner, C. G. *Angew. Chem., Int. Ed.* **1999**, *38*, 3155.
(7) Peng, X.; Manna, L.; Yang, W.; Wickham, J.; Scher, E.; Kadavanich, A.; Alivisatos, A. P. *Nature* **2000**, *404*, 59.
(8) Sun, Y.; Xia, Y. *Science* **2002**, *298*, 2176.
(9) Achermann, M.; Petruska, M. A.; Kos, S.; Smith, D. L.; Koleske, D. D.; Klimov, V. I. *Nature* **2004**, *429*, 642.
(10) Pacholski, C.; Kornowski, A.; Weller, H. *Angew. Chem., Int. Ed.* **2004**, *43*, 4774.
(11) Milliron, D. J.; Hughes, S. M.; Cui, Y.; Manna, L.; Li, J.; Wang, L.-W.; Alivisatos, A. P. *Nature* **2004**, *430*, 190.
(12) Pan, Z. W.; Dai, Z. R.; Wang, Z. L. *Science* **2001**, *291*, 1947.
(13) Goldberger, J.; He, R.; Zhang, Y.; Lee, S.; Yan, H.; Choi, H.-J.; Yang, P. *Nature* **2003**, *422*, 599.
(14) Son, D. H.; Hughes, S. M.; Yin, Y.; Alivisatos, A. P. *Science* **2004**, *306*, 1009.
(15) Sone, E. D.; Zubarev, E. R.; Stupp, S. I. *Angew. Chem., Int. Ed.* **2002**, *41*, 1706.
(16) Yang, R.; Ding, Y.; Wang, Z. L. *Nano Lett.* **2004**, *4*, 1309.
(17) Dinsmore, A. D.; Hsu, M. F.; Nikolaides, M. G.; Marquez, M.; Bausch, A. R.; Weitz, D. A. *Science* **2002**, *298*, 1006.
(18) Tang, Z.; Kotov, N. A.; Giersig, M. *Science* **2002**, *297*, 237.
(19) Park, S.; Lim, J.-H.; Chung, S.-W.; Mirkin, C. A. *Science* **2004**, *303*, 348.
(20) Yin, Y.; Rioux, R. M.; Erdonmez, C. K.; Hughes, S.; Somorjai, G. A.; Alivisatos, A. P. *Science* **2004**, *304*, 711.
(21) Wu, Y.; Xiang, J.; Yang, C.; Lu, W.; Lieber, C. M. *Nature* **2004**, *430*, 61.
(22) Penn, R. L.; Banfield, J. F. *Science* **1998**, *281*, 969.
(23) Penn, R. L. *J. Phys. Chem. B* **2004**, *108*, 12707.
(24) (a) Pacholski, C.; Kornowski, A.; Weller, H. *Angew. Chem., Int. Ed.* **2002**, *41*, 1188. (b) Cho, K. S.; Talapin, D. V.; Gaschler, W.; Murray, C. B. *J. Am. Chem. Soc.* **2005**, *127*, 7140.
(25) (a) Lou, X. W.; Zeng, H. C. *J. Am. Chem. Soc.* **2003**, *125*, 2697. (b) Sampanthar, J. T.; Zeng, H. C. *J. Am. Chem. Soc.* **2002**, *124*, 6668.
(26) Liu, B.; Zeng, H. C. *J. Am. Chem. Soc.* **2003**, *125*, 4430.
(27) Liu, B.; Zeng, H. C. *J. Am. Chem. Soc.* **2004**, *126*, 8124.
(28) Yang, H. G.; Zeng, H. C. *Angew. Chem., Int. Ed.* **2004**, *43*, 5930.


**10.1021/ja055734w CCC: $30.25** 

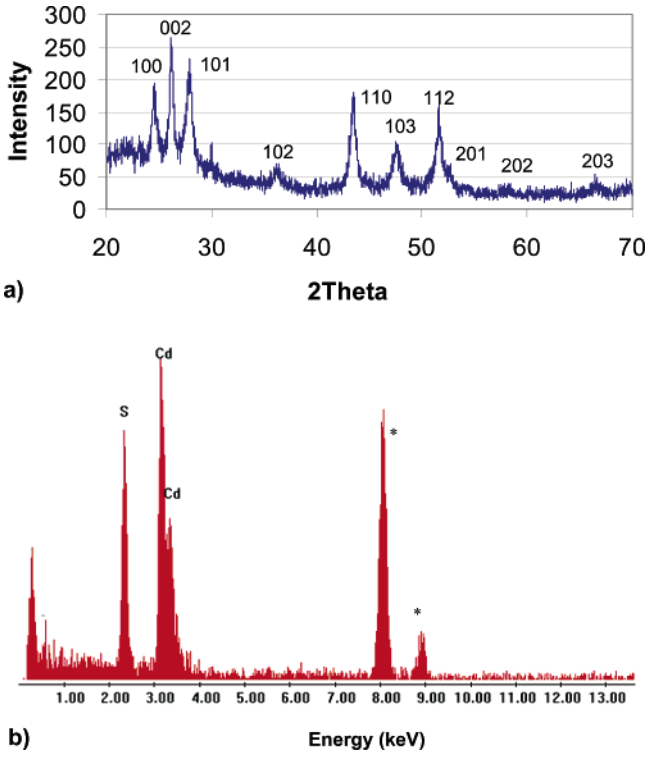


***Figure 1.*** (a) Representative XRD pattern for the wurtzite CdS samples prepared with the present approach. (b) A typical EDX spectrum obtained from an individual CdS ring. Cu signals, indicated by asterisks, were generated from a copper grid used in the EDX/HRTEM measurement.

Aldrich), or 0−0.288 g of 1,8-octanediamine (98%, Aldrich), or 0−0.232 g of 1,6-hexanediamine (98%, Sigma), or 0−0.133 mL of ethylenediamine (99%, Merck) was added to the above mixed solution. The mixture was later transferred to a Teflon-lined stainless steel autoclave and kept inside an electric oven at 150−200 °C for 4−48 h. After reaction, the autoclave was cooled to room temperature under flowing tap water. Yellow precipitates (CdS) formed from the above processes were washed several times with deionized water and pure ethanol and separated by centrifugation. The collected products were dried in a vacuum desiccator at room temperature overnight. Apart from hydrothermal reactions, synthetic experiments were also carried out at room temperature. Briefly, 0.924 g of $Cd(NO_3)_2 \cdot 4H_2O$ and 0.228 g of thiourea were dissolved in 200.0 mL of deionized water, followed by adding 0−0.5 g of ground 1,12-dodecanediamine, or 0−0.288 g of 1,8-octanediamine, or 0−0.232 g of 1,6-hexanediamine, or 0−0.133 mL of ethylenediamine to the solution. The mixed solution was then transferred to a conical flask and stirred at room temperature for 4 h, followed by the same washing and drying treatments. The thus prepared CdS samples were characterized with scanning electron microscopy, energy-dispersive X-ray spectroscopy (SEM/EDX, JSM-5600LV), transmission electron microscopy, selected area electron diffraction (TEM/SAED, JEM-2010F, 200 kV; the procedure for TEM sample preparation was similar to our previous work[28]), high-resolution transmission electron microscopy, energy-dispersive X-ray spectroscopy (HRTEM/EDX, Philips-CM200 FEG, 200 kV), and powder X-ray diffraction (XRD, Shimadzu XRD-6000, Cu Kα radiation). Light absorption spectra were collected at room temperature on a UV−vis−NIR scanning spectrophotometer (Shimadzu UV-3101PC). The photoluminescence spectra were also obtained at room temperature on a fluorescence spectrometer (C-60/200 spectrofluorometer, Photon Technology International), using xenon (310 nm) as the excitation source.

## Results and Discussion

Displayed in Figure 1, all reported CdS samples in the present work were first examined with powder X-ray diffraction (XRD) and energy-dispersive X-ray spectroscopy (both EDX/SEM and EDX/HRTEM) techniques for their crystallographic structure and chemical composition. This materials characterization shows that the prepared CdS has a wurtzite crystal symmetry and a strict stoichiometric atomic ratio (e.g., Cd/S = 1.05 based on our EDX/SEM measurement for mass samples; SG: $P6_3mc$, $a_0$ = 4.142 Å, $c_0$ = 6.724 Å; JCPDS file no. 2-549).[29] The broad XRD peaks indicate the nanocrystalline nature of the CdS samples prepared with the present approach. In particular, the strong (002) reflection, which has the highest intensity, reveals the preferred ⟨0001⟩ orientations of the CdS nanocrystallites.

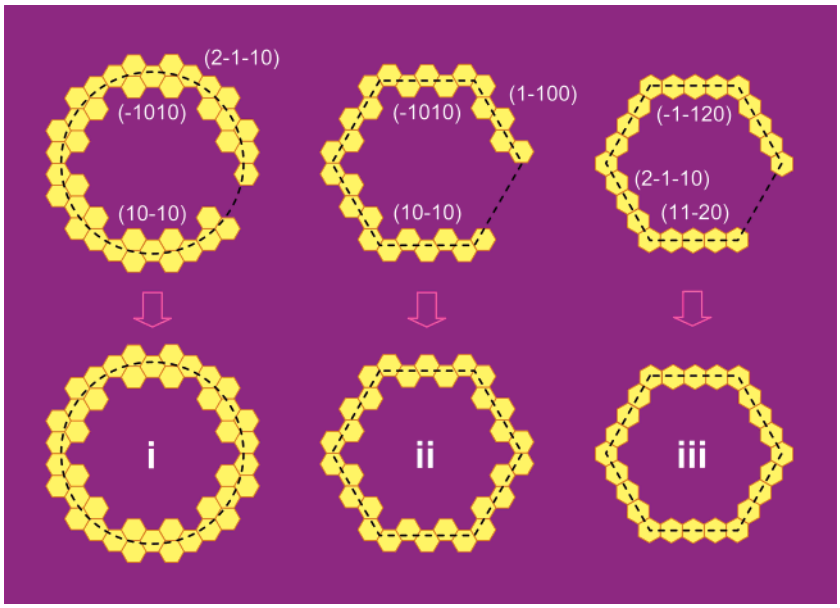


***Figure 2.*** Schematic illustration of three novel self-tuning mechanisms for ring formation (viewed along the [0001] axis of the wurtzite CdS crystal): (i) a circular ring arrangement formed from hexagonal nano building blocks with alternative crystal plane segments of the {10−10} and {11−20} families, (ii) a hexagonal ring bound with low-Miller-index crystal planes of the {10−10} family, and (iii) a hexagonal ring bordered with higher-Miller-index crystal planes of the {11−20} family. Some of the inner or outer crystal planes are indicated to show correlations among the structures (refer to the later figures for actual product morphologies).

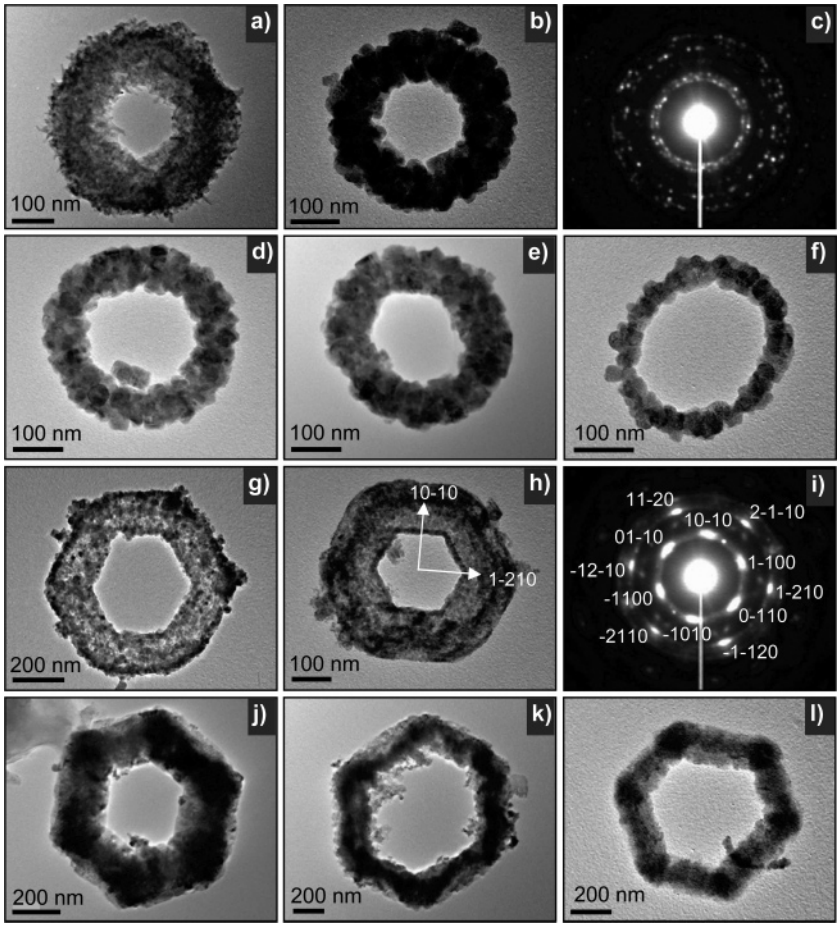


***Figure 3.*** TEM images of the type (i) circular CdS rings (a−f) and of the type (ii) hexagonal CdS rings (g−l). The SAED patterns in (c), a polycrystalline diffraction pattern, and (i), a single-crystal-like [0001] zone diffraction pattern, were measured for the rings in the images (b) and (h), respectively.

Figure 2 illustrates three types of ring organization starting from 0D building blocks.[30] The first type (i) of organization is based on the 6-fold symmetry of wurtzite CdS {0001} surfaces. An idealized hexagonal building unit would have six equal chances to attach its neighboring crystallites, and a statistical assembly of the tiny hexagons may give rise to the formation of a curvature if some of the planes are interconnected. The second type (ii) and third type (iii) of organization, on the other hand, are more rigidly attained upon some specific crystallographic requirements, in which the hexagonal crystallite units are aligned along the ⟨11−20⟩ and ⟨10−10⟩ directions, respectively. Unlike the type (i) circular structure, the type (ii) and (iii) rings are formed with straight segments as a result of the directional alignments. Regarding the latter two cases, it should be mentioned that among the polygons related to the known crystal systems, the hexagon possesses the highest rotational symmetry and gives the best approximation to circular structures.

The perfect hexagonal crystallite units with an identical size drawn in Figure 2 are merely for illustrative purpose. In reality, the nanocrystallites that construct the rings are not necessitated to have a perfect hexagonal shape and to be in an equal size. In principle, ring-forming attachment can proceed as long as the CdS crystallites possess a certain amount of {10−10} and

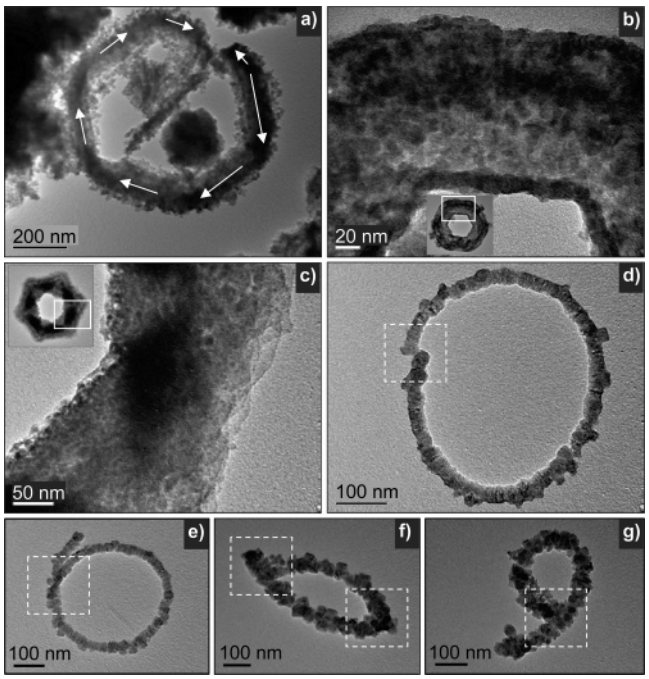


***Figure 4.*** TEM images of (a) an intermediate hexagonal ring structure; the white arrows indicate the propagating directions of the CdS crystallite assembly. (b and c) Detailed views of the ring structures; the solid white frames of the insets indicate the examined areas. (d−g) Incomplete circular ring structures with larger crystal units; the dashed white frames show the mismatching parts of ring closure.

(29) Barrelet, C. J.; Wu, Y.; Bell, D. C.; Lieber, C. M. *J. Am. Chem. Soc*. **2003**, *125*, 11498.

(30) In this text, the {10−10} family includes (10−10), (−1010), (01−10), (0−110), (1−100), and (−1100) crystal planes; the {11−20} family includes (11−20), (−1−120), (1−210), (−12−10), (2−1−10), and (−2110); and the {0001} family comprises (0001) and (000−1).

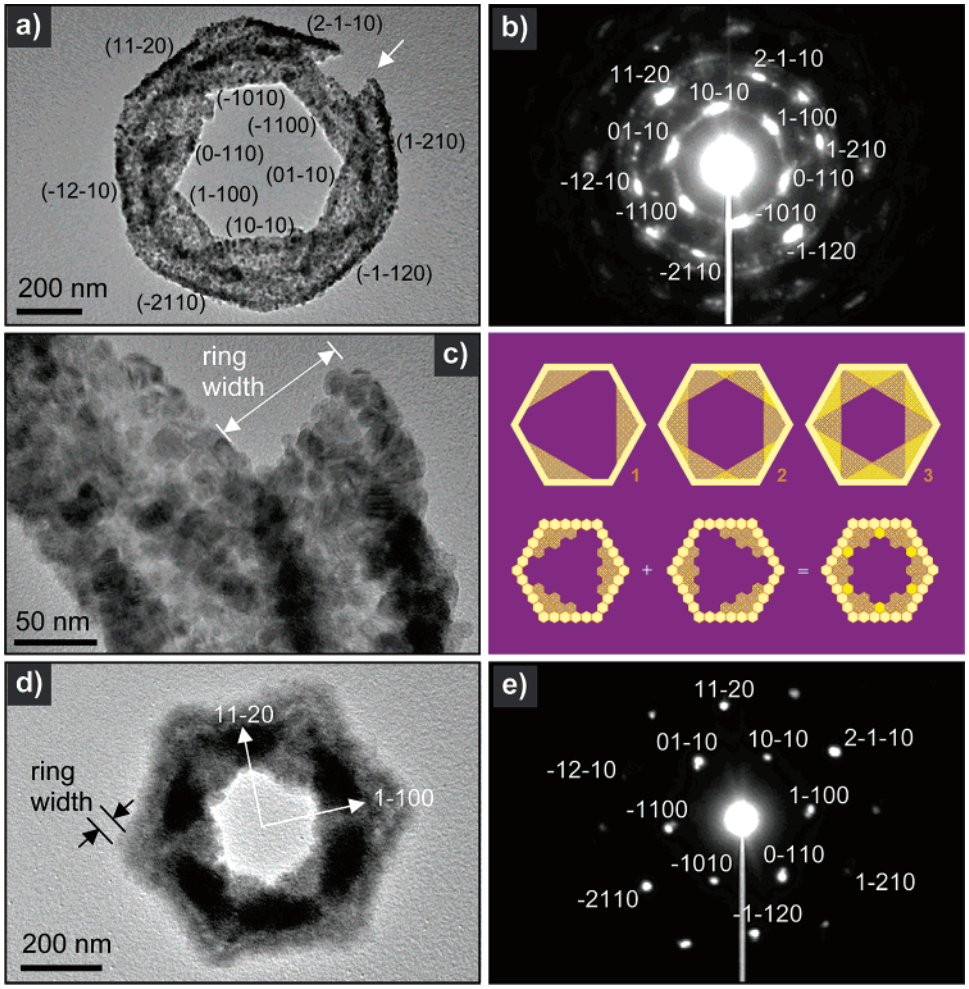


***Figure 5.*** TEM images of the type (iii) hexagonal CdS rings (a, c, and d). The SAED patterns ([0001] zone diffraction spots) of (b) and (e) were measured for the rings in the images (a) and (d), respectively. Image (c) is a magnified part of (a) showing a chipped area of the initial ring structure whose breadth is marked with a white arrow. This inward planar attachment starts, respectively, at six corners of a preformed hexagonal ring. The color inset illustrates this process in separate steps for visual clarity: (1) starting at three corners; (2) starting at all six corners; (3) continuous in-plane growth. Note that there are six overlapping regions shown as light-yellow parts in this illustration.

{0001} planes or facets on their external surfaces, even their shape and size are polydispersed. All the above three types of organizing schemes have been actually observed in the present work. In Figure 3a−f, CdS rings assembled with scheme (i) are displayed. As can be seen, the circular structures were built from smaller crystallites; their crystal size depends on actual experimental conditions. In general, a higher synthetic temperature leads to better crystallinity, but larger sizes, for the products. Since the orientation requirement is less stringent in these cases, a crystallite can use one or several of its six lateral crystal planes in the ring development. Due to this, the degree of disorientation among the participating crystallites is higher. Apart from the horizontal ring formation with the {10−10} planes or facets, the CdS nanocrystallites can also used their {0001} planes, where $Cd^{2+}$ cations are rich on the positive plane/facet (0001) and $S^{2-}$ anions are rich on the negative plane/facet (000−1), for a stacking along the ⟨0001⟩ axis. This vertical "oriented attachment" results in an increase in the thickness of nanostructures, as evidenced in all the CdS rings prepared (e.g., the TEM images in all figures). In a later stage of ring thickening, however, some crystallites might also be deposited randomly onto the ring structures. The study with selected area electron diffraction (SAED) in Figure 3c indeed reveals the polycrystalline nature for the CdS ring comprised of large crystals. Although the stacking along the ⟨0001⟩ axis has been observed, it is known that the {0001} planes are relatively inactive, compared to their other crystal planes under the current experimental setting, on the basis of the XRD/SAED/TEM/HRTEM investigations. This point will also be further addressed in the later part of this work.

The hexagonal rings were also constructed from a sequential self-assembly process, as indicated by some crystal intermediates shown in Figure 4a, noting that the left-hand-side part is thinner than the right-hand-side one (i.e., the starting part). As regards the turning observed, it is assumed that any growth perturbations could eliminate the straight 1D growth and initiate a turning. This postulation is based on the facts that the lengths on hexagonal rings are not exactly identical in some cases (Figure 3g−l) and there is a maximum limit for the 1D segments; only short nanorods were formed under such experimental conditions (see Figure 7a later). The rings assembled with the type (ii) organization are shown in Figure 3g−l. In these ripened rings, the inner hexagonal space follows strictly the external hexagonal frame. Compared to type (i) rings, the crystallites in the type (ii) are generally finer, as detailed in Figure 4b (also refer to Figure 3h); it is believed that small-sized crystallites may have more steric freedom during their oriented aggregation in solution medium. Figure 3i presents a single-crystal-like diffraction

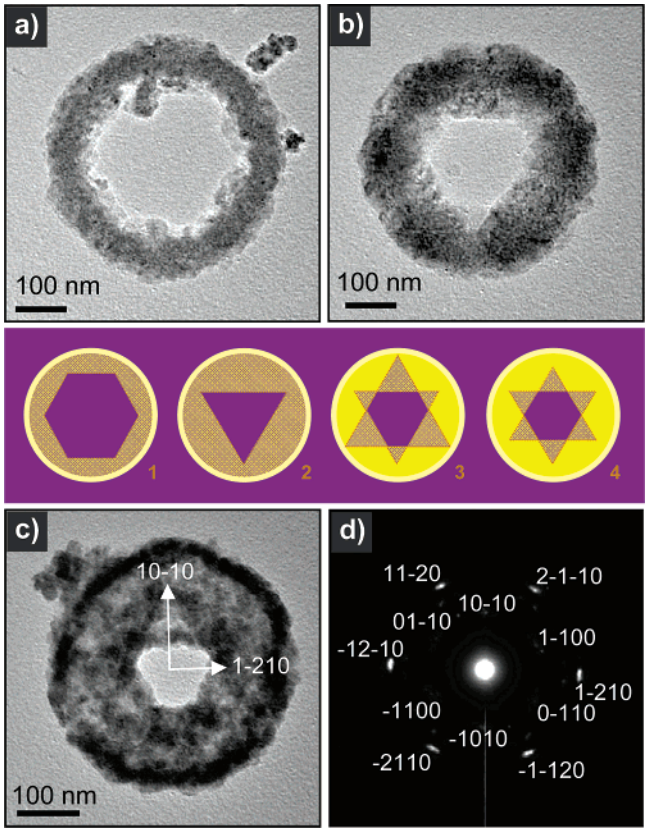


***Figure 6.*** TEM images of the type (i) circular CdS rings (a−c). The SAED pattern ([0001] zone diffraction spots) in (d) was measured for the ring shown in (c). The color inset illustrates an in-plane attachment process of nanocrystals: (1) a circular ring centered with a hexagonal inner space; (2) three crystal planes propagating at a fast growth rate; (3) two sets of crystal planes formed due to different growth rates; (4) all six crystal planes grown at the same growth rate. The process is essentially similar to that illustrated in Figure 5 but with starting points from a preformed circular ring (see the main text).

pattern, indicating that a unified global crystallographic relationship among the crystallites on the ring is maintained. The type (ii) organizing scheme can be thus confirmed unambiguously.

Compared to the type (ii) organization, the rings formed in accordance to the type (iii) scheme are less populated. The population ratios among the types (i), (ii), and (iii) rings are approximately 60%, 30%, and 10%, respectively (based on a total of 243 TEM images), noting that the statistical ratios vary upon different experimental conditions. Although the type (iii) CdS rings are bounded with apparent crystal planes of {11−20}, microscopically, individual crystallites are still faceted with the same low-Miller-index planes of {10−10} (Figure 2iii). Therefore, no appreciable variation in surface energies in the outer boundaries of type (iii) rings should be expected. In addition to the initial {11−20} boundaries on the hexagonal rings, quite interestingly, there is also a possibility for coexistence of the {10−10} planes. In Figure 5, an inward ring growth produces an inner hexagonal space which is 30° away from its external hexagonal framework. The central hollow hexagon is indeed terminated with six {10−10} planes, as revealed in the single-crystal-like SAED pattern of this CdS structure. The type (iii) organizing scheme (Figure 2) is thus affirmed. In light with the resultant overlapping areas, it is clear that the in-plane oriented attachment of the crystallites proceeds at every corner of the hexagonal ring simultaneously (Figure 5, parts a and c). The crystallite sizes are in the range of 5−20 nm (e.g., 10−20 nm in Figure 5c). This evolving process is also schematically illustrated in Figure 5. As a further confirmation, an almost perfect ring comprised of even smaller crystallites is displayed in Figure 5d (also refer to Figure 4c). In excellent agreement with the described growth process, there are exactly six dark triangles observed on the ring that correspond to the overlapping areas (structure 3, inset of Figure 5); one of the six areas of this ring can be further examined in Figure 4c.

While all the three types of organization schemes show the preferred planar orientations of ⟨0001⟩, it should be stressed that the main difference among them is the lateral orientation of the basic segments that build the rings. For the hexagonal rings depicted in Figure 2, the predominant (edge) segments are either {10−10} (type ii) or {11−20} (type iii) except for the small corner areas which belong to {11−20} and {10−10}, respectively. Nonetheless, in the type (i) rings, both segments of {10−10} and {11−20} should have a similar statistical proportion. Furthermore, they should also be connected in an alternative manner in order to ensure a smooth curvature development. If this is not the case, the aggregation process will run out of a circumferential track, and the ring would be distorted (e.g., an oval ring in Figure 3f). In fact, as indicated in Figure 4d−g, perfect ring closure is always a problem for the rings formed by only a few large crystal units, even though the individual crystallites are fused without violating the rules of oriented attachment.[22,23] If the crystallites in this type of ring are small, however, further in-plane crystallite aggregation can still proceed as illustrated in Figure 6. Starting with a circular ring, an inward attachment of nanocrystallites gives rise to the formation of a hexagonal space (Figure 2i and Figure 6a) with {10−10} growth fronts. It is understandable that, due to the starting structural inhomogeneity, the growth rates of all the crystal planes in an inner ring are not necessarily the same. As a result, these crystal planes might further differentiate themselves into different sets. In Figure 6, parts b and c, this in-plane growth led to the formation of two inversed triangles at 180° apart. The edge lengths of the inner hexagon are not equal (structure 3, inset, and Figure 6c), suggesting that the growths were commenced at different times or at different rates. For this type of ring, excellent matching among the crystallites can still be attained if they are small, as evidenced in single-crystal-like diffraction patterns (Figure 6d).

Most of the TEM images reported above are not of high resolution, and the image contrasts in the grain boundary areas (at lighter contrasts, e.g., Figure 5c) can sometimes be misleading. As a further confirmation, Figure 7 shows a hexagonal ring together with its lower-dimensional building blocks. Interestingly, many nanocrystallites have readily attached into straight rodlike structures. It is thus observed that these 1D crystals worked as starting segments for the integration of 0D crystallites and the formation of hexagonal frameworks. In Figure 7b, three crystallites in a ring structure are displayed. Consistent with the organizing schemes of Figure 2, these nanocrystals are primarily faceted with the {10−10} crystal planes, noting that lattice fringes of $d_{10-10}$ (0.36 ± 0.01 nm) can be observed in all crystallites; the hexagonal shape of CdS crystallites can also be seen clearly in Figure 8c. Crystallographically, the attachment between the primary crystallites 1 and 2 is almost perfect, while crystallite 3 is slightly misoriented. The mismatching in the latter

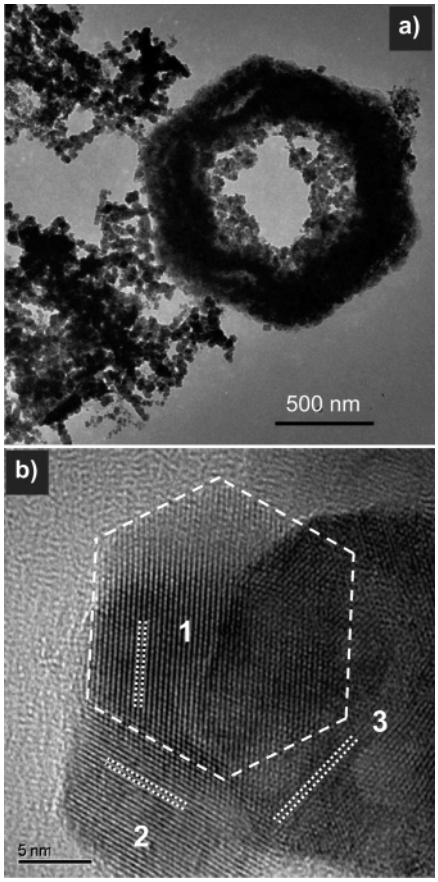


***Figure 7.*** (a) TEM image of a hexagonal CdS ring with the type (ii) assembling scheme, together with its starting 0D and 1D building units. (b) An HRTEM image which shows orientations and lattice fringes of three neighboring crystallites (1−3). The dashed hexagonal frame shows the boundary area of the crystallite 1. Dotted double lines indicate the lattice spacing of $d_{10-10}$. Misorientation among the three crystallites can also be measured from the angles between these paired lines.

cannot be entirely avoided as long as there are unequal sizes and/or uneven surfaces in these 0D building units. This explains the origin for the elongation of the diffraction spots observed in the SAED patterns. To further verify these findings, three HRTEM images (a−c) in Figure 8, together with Figure 7b, reveal that all CdS crystallites that build the ring structures are indeed well integrated according to the "oriented attachment" mechanism.

In addition to the HRTEM confirmation, we should also rule out the possibility that the observed ring formation is caused by simple drying.[31] In comparison, the CdS rings formed in the present work are fundamentally different from a template-supported ring formation of Ag nanoparticles.[31] Although crystallite grain boundaries can be observed in our TEM study (which is the direct evidence for oriented attachment), there are no intercrystallite spaces among the CdS crystallites (HRTEM result, see Figures 7 and 8). In contrast, the discrete dotlike Ag nanocrystals (2.5 nm in size), which form circular ring structures, are well separated from each other with a constant interparticle space of about 2.0−2.5 nm (owing to the capping of dodecanethiol surfactant on the Ag surfaces), and their single-layer ring structures can only be formed with the TEM sample grid surface as a template during the drying.[31] On the other hand,

(31) Ohara, P. C.; Heath, J. R.; Gelbart, W. M. *Angew. Chem., Int. Ed. Engl.* **1997**, *36*, 1077.

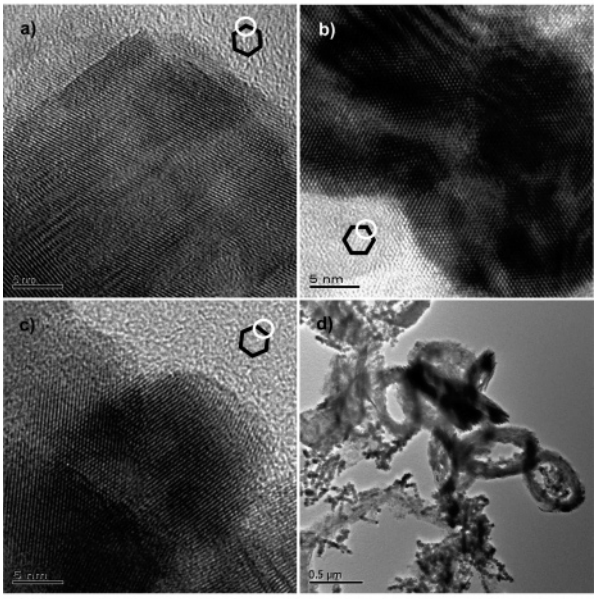


***Figure 8.*** HRTEM images (a−c) detail the fine structures of different areas of the CdS ring. White circles illustrate the location of a ring in this HRTEM investigation. The TEM image (d) shows a bunch of CdS rings standing on the TEM sample grid, which rules out the possibility of a surfactant-assisted or grid-template-assisted formation mechanism.

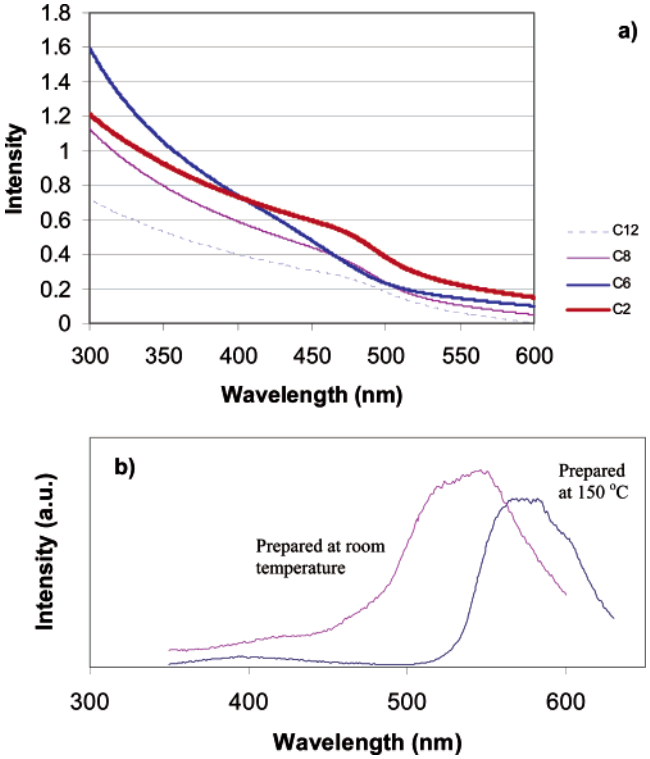


***Figure 9.*** (a) Representative absorption spectra of CdS samples prepared at room temperature. C*n* indicates the diamines used in the synthesis: C12 = 1,12-dodecanediamine, C8 = 1,8-octanediamine, C6 = 1,6-hexanediamine, and C2 = ethylenediamine. (b) Room-temperature photoluminescence spectra of CdS samples prepared at two different temperatures. Measurement conditions: 0.01 g of sample was dispersed in 3.5 mL of pure ethanol. During the measurements, 2 drops of the above dispersed solution was added to a quartz cell holder filled with pure ethanol. The total volume of the liquid was around 4 mL.

the crystallites in our CdS ring structures are fully integrated and continuous; they can stand rigidly at various angles with respect to the TEM sample grid (Figure 8d), which excludes

the possibility of a surfactant-assisted or grid-template-assisted formation mechanism. Furthermore, the as-prepared samples from our syntheses were washed thoroughly and dried (see the Experimental Section), and all residual amines were removed completely from the samples prior to a redispersion in preparations of suspension for TEM measurement. Therefore, formations of vesicles and micelles for organization of nanoparticles during the drying of TEM suspensions can also be ruled out unambiguously.

Our UV−vis absorption measurements, shown in Figure 9a, and optical band gap calculation indicate a direct transition $E_g = 2.45-2.48$ eV for the CdS samples prepared in this work. Consistent with the observed crystallite size, the calculated optical band gaps are only slightly larger than that of the bulk value (2.42 eV),[32] as all assemblies created herein had led to crystal enlargement although our starting building units were in the nanoscale regime. In agreement with the XRD/TEM/HRTEM results, our CdS samples also exhibit size-dependent behavior. For the sample prepared at room temperature (at smaller sizes), the photoluminescence peak is located at about 530 nm, whereas for the sample prepared at 150 °C, the peak is shifted to 580 nm (Figure 9b).[32]

Concerning the use of diamines in the above synthetic architecture, three basic roles can be identified: providing basic media for decomposition of thiourea ($(NH_2)_2CS + 2OH^- \rightarrow CH_2N_2 + 2H_2O + S^{2-}$), stabilizing the {0001} planes, and chelating agents to cadmium cations in either the liquid phase or the solid phase. Although all diamines used in this work (1,12-dodecanediamine, 1,8-octanediamine, 1,6-hexanediamine, and ethylenediamine) produce ringlike structures, the long-chained 1,12-dodecanediamine gives the highest yield of rings (about 20%, using our growth parameters). This observation may be attributed to a spatial flexibility of long-chained diamines in chelating cadmium cations in different neighboring crystallites. In a simple analogy, these bidentate ligands may act as "staples" in pulling free-standing crystallites together prior to the oriented aggregation taking place in the liquid medium. Further in-depth investigation in this mechanistic aspect will be carried out soon.

As most semiconducting materials can have rather similar crystal symmetries, in principle, the processes revealed in this work should be extendable to other semiconductors. For example, groups IV (e.g., Si) and III−V (e.g., GaAs) semiconductors have cubic symmetry, and by controlling the ⟨111⟩ orientations a 6-fold symmetry similar to that in wurtzite ⟨0001⟩ (i.e., Figure 2) can also be attained. As for the groups II−VI (e.g., ZnS and CdS), two common crystal systems are known, zinc blende (which also belongs to cubic symmetry) and wurtzite (hexagonal, the current work) structures. The immediate research task in this area, therefore, should be directed to the investigation of ring formation for the materials with a cubic crystal symmetry.

## Conclusions

In summary, three types of lateral organization schemes for creating ringlike structures have been elucidated with the self-assembly of nanocrystals. The synthetic architecture is based on morphological controls of primary nanocrystals which possess an intrinsic hexagonal symmetry. By stabilizing suitable crystal planes, such as the {001} planes for the hexagonal crystal system and the {111} planes for the cubic crystal system, the principles and schemes established in the present self-assembling study should be extendable to other semiconductor nanocrystals in oriented construction of their ring structures.

**Acknowledgment.** The authors gratefully acknowledge the financial support of the Ministry of Education, Singapore.

JA055734W

(32) (a) Yu, W. W.; Peng, X. *Angew. Chem., Int. Ed.* **2002**, *41*, 2368. (b) Trindade, T.; O'Brien, P.; Pickett, N. L. *Chem. Mater.* **2001**, *13*, 3843.